A Green and Sustainable Approach for Acetalization of Benzaldehyde Using Tungstophosphoric Acid Loaded on Metal Oxide Catalysts

[1]Li Fanghao, [1]Li Chenjie, [1]Chen Junyi, [1]Wang Kuiwu, [2]Zhang Haijiang, [1]Wang Yanbo and [1]Han Xiaoxiang
[1]Department of Applied Chemistry, Zhejiang Gongshang University, Hangzhou 310018, China
[2]Jiangsu Key Laboratory of Regional Resource Exploitation and Medicinal Research, Huaiyin Institute of Technology, Huaian 223003, China.
wyb1225@163.com*

(Received on 20th April 2018, accepted in revised form 31st January 2019)

Summary: A series of tungstophosphoric acid ($H_3PW_{12}O_{40}$; HPW) loaded on metal oxide catalysts, namely $H_3PW_{12}O_{40}$/M (M= TiO_2, CeO_2, ZrO_2) was prepared by initial wetting impregnation method and their catalytic performances were also investigated during the condensation reaction of benzaldehyde with glycol. Among them, the 20 wt% $H_3PW_{12}O_{40}/TiO_2$ catalyst demonstrated highly active with superior acetal yield (90.1 %) and excellent durability. The high activity of the catalyst derived from high surface area, ultra-strong Brønsted acidity and synergetic effect of Brønsted-Lewis acid. Response surface methodology (RSM) based on Box-Behnken design (BBD) was used to optimize the course of the condensation reaction of benzaldehyde with glycol, and the optimal benzaldehyde glycol acetal yield (93.4 %) could be obtained. The optimized yield and the experimental results are similar. Moreover, under optimal reaction conditions, the activation energy (*Ea*) of reaction could be obtained through the kinetic study of the irreversible parallel reaction model, and the *Ea* was 23.24 kJ/mol.

Keywords: Titania, Heteropolyacid, Acetalization, Process optimization.

Introduction

Acetals that are commonly as new high-grade spices and important synthetic intermediates are extensively used in food fragrance daily flavor and organic synthesis [1-4]. As carbonyl derivatives, acetals are often used to protect carbonyls during the synthesis of many fine chemical products [5-9]. Typically, Homogeneous acid catalysts are often used in acetalization. However, overuse of these homogeneous acid catalysts leads to both corrosion of the equipment and polluted environment. Concurrently, with the development of society, people put forward better higher requirements to the quality of essence and environmental protection [10, 11]. Thus, a great deal of research efforts have been undertaken, of which the development of new environmentally friendly green catalyst has gained considerable attention in recent years. In this context, heteropolyacids are representative of environmentally friendly catalysts. Among them, heteropolyacids with Keggin-type structure, which owns distinct features such as higher catalytic activity, strong acidity, redox, 'quasi-liquid phase' behavior, and multifunction, have been widely utilized for olefin epoxidation, acetal reaction, etc [12-17]. Nonetheless, owing to their low surface area and recovery difficulties is limited its application in the field of catalysis [18-21]. Accordingly, heteropolyacids are often loaded onto porous materials or are made into insoluble heteropoly salts (metal or heteroatom substituted HPAs), yet particles of heteropoly salts employed in heterogeneous or homogeneous reactions was too small to be separated in the liquid solid system [22-24]. As such, it is highly desirable to load HPA on high surface area available carrier and solve the aforementioned problems and effectively disperse phosphotungstic acid, improve the catalytic activity and stability [25-30]. In addition, on the choice of carrier, researchers have generally selected molecular sieves, activated carbon, attapulgite, etc. Recently, metal oxides also have been found as catalysts or supports, and widely used in various fields. For example, Astam K. Patra, et al. synthesized a highly ordered two-dimensional (2D) hexagonal TiO_2-Fe_2O_3 mixed oxide material MFT-1with large surface area by sol-gel method. The oxide showed excellent catalytic activity and reusability in the aromatic dehalogenation experiment [31]. The catalyst of heteropolyacids supported by metal oxide also showed good catalytic properties [21, 32]. The synergetic effect of Brønsted acid (H^+ from heteropolyacids) and Lewis acid (metal ion) was responsible for it. A 93.6 % combined selectivity of glyceryl triacetate and glyceryl diacetate with complete glycerol conversion was obtained in the presence of $HSiW/ZrO_2$ [32]. The 20 wt% HPW/CeO_2 catalyst showed high benzaldehyde yield (94.2 %) for liquid phase oxidation of benzyl alcohol with hydrogen peroxide [21].

Based on our laboratory study, a series of tungstophosphoric acid ($H_3PW_{12}O_{40}$; HPW) loaded on

*To whom all correspondence should be addressed.

metal oxide catalysts were produced through initial wetting impregnation method, among them, Titanium dioxide supported phosphotungstic acid has the best catalytic effect. Then these techniques (FT-IR, XRD, BET and solid-state ^{31}P magic angle spinning (MAS) NMR) were used to characterize the catalyst. Moreover, in order to low-cost, large-scale production of acetal to provide basic data, applying response surface method to optimize the process conditions and under this optimized conditions to study the dynamics of acetal reaction. Various techniques are then used to characterize the catalyst.

Experimental

Materials and catalyst preparation

TiO_2, CeO_2, ZrO_2, SnO_2, benzaldehyde, glycol, cyclohexane, tungstophosphoric acid ($H_3PW_{12}O_{40}$; HPW) and other chemicals were analytical grade and were commercially available without further purification unless otherwise specified.

All HPW supported on metal oxide catalysts were synthesized by conventional impregnation method. Typically, the 20 wt% HPW/TiO_2 catalyst was prepared by impregnation of 3.0 g titania support with an aqueous solution of HPW. The loading of HPW is 10-25 wt%. The sample was impregnated for 12 h, dried at 393 K overnight, and then calcined at 423 K in static air for 4 h. Similar method was utilized to compound other catalysts, as listed in Table-1. All reported data in Table 1 were average results from three parallel runs.

Table-1: Catalytic performances of different catalysts on the acetalization of benzaldehyde with glycol[a].

Catalyst	Conversion (%)[b]	Selectivity (%)[b]	Acetal yield (%)[c]
TiO_2	Nil	Nil	Nil
$H_3PW_{12}O_{40}$	69.6	98.1	68.3
10HPW/TiO_2	87.0	98.3	85.5
15HPW/TiO_2	88.5	98.7	86.7
20HPW/TiO_2	91.4	98.6	90.1
25HPW/TiO_2	77.1	98.4	75.9
20HPW/ZrO_2	66.4	99.1	70.8
20HPW/CeO_2	79.1	98.6	78.0

[a] Reactions conditions: glycol : benzaldehyde of 1.6 mol/mol; 6 wt% of catalyst amount; 3 h; 12 mL of cyclohexane; temperature = 383 K.
[b] Analyzed by GC.
[c] Analyzed by distillation. An experiment error of less than 1% compared to GC analyses can be inferred.

Catalyst characterization

All Fourier-transform infrared (FT-IR) spectra for HPW/TiO_2 catalysts in KBr disks were recorded on a Bruker IFS-28 spectrometer in the range of 4000–400 cm^{-1} region. X-ray diffraction (XRD) characterization was carried out on Rigaku Ultimate IV, and the tube current and tube voltage were 40 kV and 40 mA, respectively. Under the 2θ angle range of 5-80° with a scanning rate of 10°/min condition, the XRD patterns were recorded. The N_2 adsorption experiments that were occurred at 77 K on a Quantachrome Autosorb-1 apparatus were employed to determine surface areas of the supported HPW catalysts. The Brunauer- Emmett-Teller (BET) method was applied to derive the total surface areas of the samples. The acidity of the supported HPW catalysts were characterized by means of a ^{31}P-TMPO MAS NMR approach in Bruker Avance III 500 type NMR apparatus. The ^{31}P MAS NMR spectra were measured at a Larmor frequency of 202.46 MHz using a single-pulse sequence under a sample spinning rate of 12 kHz. The excitation pulse for ^{31}P was 1.5 (π/6) and the recycle delay was 10.0 s. The chemical shifts of ^{31}P ($\delta^{31}P$) were referenced to that of 85 % H_3PO_4 aqueous solution. The detail of sample processing was prepared following the procedure outlined in literature [33, 34].

Catalytic reaction

The typical acetalization procedure followed was: benzaldehyde (10.6 g, 0.1 mol), ethylene glycol (9.9 g, 0.16 mol), catalyst (0.6 g) and water carrying agent (cyclohexane, 12 mL) were put in a 100 mL three-necked flask. The flask equipped with a water separator, a stir bar and a reflux condenser. The reaction mixture was stirred under reflux for a desirable period of time in an oil bath. Upon completion, the reaction mixture was cooled to RT and the layers separated. The organic layer was quantitatively analyzed by gas chromatography (Agilent 7890B) with a FID detector and an HP-5 capillary column. Reactants and products are confirmed by comparing with authentic samples using biphenyl as the internal standard. The 497~501 K fraction for the yield of acetal was collected by atmospheric distillation. The product is liquid with fruity aroma and colorless transparent. Meanwhile, the catalyst was thoroughly washed with diethyl ether for the recyclability tests.

Experimental design and mathematical model

The optimum conditions for the synthesis of benzaldehyde glycol acetal using 20 wt% HPW/TiO_2 as catalyst were determined by means of response surface methodology. The relationship between yield of acetal with molar ratio of glycol/ benzaldehyde (x_1), reaction time (x_2), amount of catalyst (x_3) and amount of water-carrying agent (x_4) was evaluated by

Box-Behnken design experiment.

According to the Box-Behnken design principle, all the single factors in the experiment are encoded as three levels, namely -1, 0 and +1 as shown in Table-2 and 29 sets of experiments including 24 factorial points and 5 central points (Table 3) were adopted. The response of the experimental design, denoted *Y*, may be expressed as follows:

$$Y = \beta_0 + \sum_{i=1}^{k} \beta_i x_i + \sum_{i=1}^{k} \beta_{ii} x_i^{\,2} + \sum_{j=1}^{k} \beta_{ij} x_i x_{ij} + \varepsilon \quad (1)$$

where x_i and x_j (i & j = 1–k) represented uncoded independent variables, β_0, β_i, β_{ii}, and β_{ij} were the regression coefficients representing the offset term, main, quadratic, and interaction effects, respectively; k was the total number of design variables; ε was the random error.

Table-2: Actual and corresponding coded values of each parameter.

Variables	Symbol	Levels		
		-1	0	1
Molar ratio Glycol to benzaldehyde	x_1	1.4	1.6	1.8
Reaction time (h)	x_2	2.5	3	3.5
Amount of catalyst (wt%)	x_3	5	6	7
Amount of cyclohexane (mL)	x_4	10	12	14

Kinetic study

The reaction rate equation for the acetal reaction can be expressed as:

$$r = -\frac{dC_A}{dt} = k_+ C_A^{\,\alpha} C_B^{\,\beta} - k_- C_C^{\,\gamma} C_D^{\,\eta} \quad (2)$$

where r is the reaction rate of the reaction of benzaldehyde with ethylene glycol. k_+ and k_- are the forward and reverse rate constants, respectively; C_A, C_B, C_C and C_D are the instantaneous concentrations of benzaldehyde, ethylene glycol, acetal and water. α, β, γ and η are their reaction order.

Given that water had been effectively removed by water-carrying agent (cyclohexane) during the acetalization reaction, the reaction could be considered as an irreversible process. Under these conditions, the second term associated with the inverse process in eqn (2) may be ignored. The reaction rate equation (2) can be simplified as:

$$r = -\frac{dC_A}{dt} = kC_A^{\,\alpha} C_B^{\,\beta} \quad (3)$$

For simplicity, assuming that forward for substrate are both first-order (α=β=1) and $Q = C_{B0}$-C_{A0}. Among them, C_{A0} is initial concentration of benzaldehyde (mol/L), C_{B0} is initial concentration of ethylene glycol (mol/L), then $C_{B0} = C_A + Q$. Equation (3) can be rewritten as:

$$r = -\frac{dC_A}{dt} = kC_A(C_A + Q) \quad (4)$$

Taking the natural logarithm, eqn (4) may further be expressed as:

$$\ln\frac{C_A + Q}{C_A} = Qkt + C \quad \text{or} \quad \ln\frac{C_A}{C_B} = (C_{AO} - C_{BO})kt + C \quad (5)$$

The values of k and C for the acetalization reaction at different temperature could be obtained by performing linear fitting for the relationship between ln C_A/C_B with t through Origin 8.0. The variation of reaction rate with temperature may be expressed by the Arrhenius equation as:

$$\ln k = \ln k_0 - \frac{E_a}{R}\frac{1}{T} \quad (6)$$

Thus, the pre-exponential factor (k_0) and the activation energy (Ea) may be derived from the slope and the intercept of the Arrhenius (ln k vs. 1/T) plot.

Results and Discussion

Structural analysis of HPW loaded on metal oxide catalysts

The FTIR spectra of HPW, TiO_2 and HPW/TiO_2 with different loading of HPW were recorded in the Supplementary Information (Fig. S1). As shown in Fig. S1a, pristine HPW had four typical Keggin structural peaks in the range of 700-1100 cm^{-1}, which were the asymmetric stretching vibrations of P-O at 1080 cm^{-1}, terminal W=O at 983 cm^{-1}, corner-sharing W-O_b-W at 889 cm^{-1} and

edge-sharing W-O_c-W bonds at 804 cm^{-1}. [35, 36]. Similar to the pristine HPW, four typical peaks appeared distinctively in HPW/TiO_2 catalyst with different loading of HPW, even though peak intensities declined and absorption center offset slightly (Fig.S1c–e). The overlapping wide absorbance peak at ca. 3435 cm^{-1} was related to the stretching vibrations of O–H. Peaks at 598 cm^{-1} related to symmetric vibrations of O–P–O and 516 cm^{-1} may be contributed to W–O–W. The above results indicated that structure of Keggin type in the *x* HPW/TiO_2 (*x* = 10, 15, 20 and 25 wt%) were preserved well.

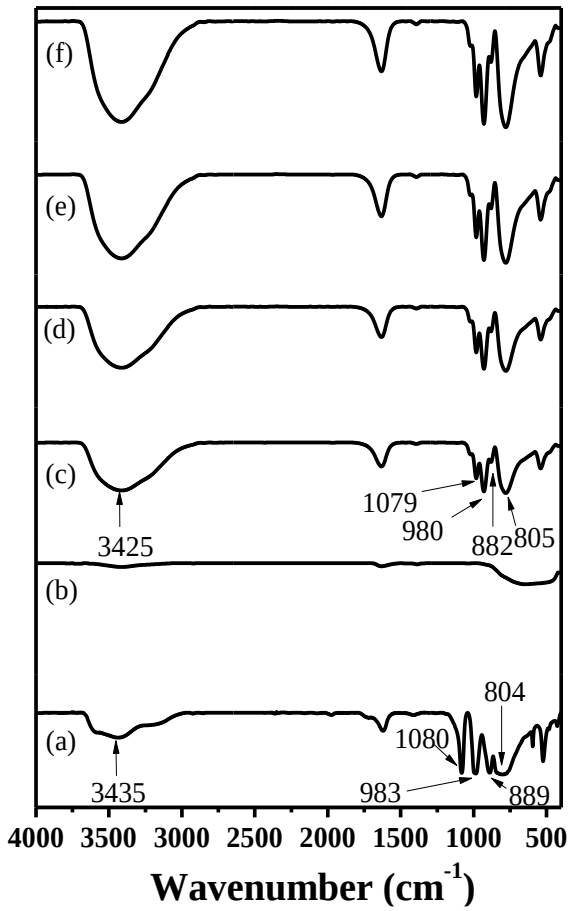

Fig. S1: FT-IR spectra for different loading HPW on TiO_2 catalysts and pure phosphotungstic acid, (a) $H_3PW_{12}O_{40}$, (b) TiO_2, (c) 10 wt% HPW/TiO_2, (d) 15 wt% HPW/TiO_2, (e) 20 wt% HPW/TiO_2 and (f) 25 wt% HPW/TiO_2.

Fig. S2 (Supplementary Information) presented XRD patterns of TiO_2, HPW and *x* HPW/TiO_2 (*x* = 10, 15, 20 and 25 wt%) catalysts. As shown in Fig.S2a, TiO_2 carrier showed XRD profile with evident diffraction peaks at 2θ angles of 25.26º(101), 37.81º(103), 48.02º(200), 53.98º(105), 55.08º(211), 62.15º(213), 62.71º(204), 68.2º(116), 70.32º(220), 74.97º (215), respectively. The diffraction peaks of as-prepared TiO_2 are in agreement with the TiO_2 anatase structure (JCPDS 21-1272). In addition, it was unable to observe the characteristic diffraction peaks of HPW related to the PW Keggin element at 10.3, 25.3, and 34.6º, in various supported *x* HPW/TiO_2 (*x* = 10, 15, 20 and 25 wt%) [37]. We also found that XRD curves of these HPW loaded on metal oxide catalysts were similar to the as-prepared TiO_2. The XRD results indicated that the HPW species of series HPW/TiO_2 catalysts were finely and molecularly dispersed on the surface of TiO_2.

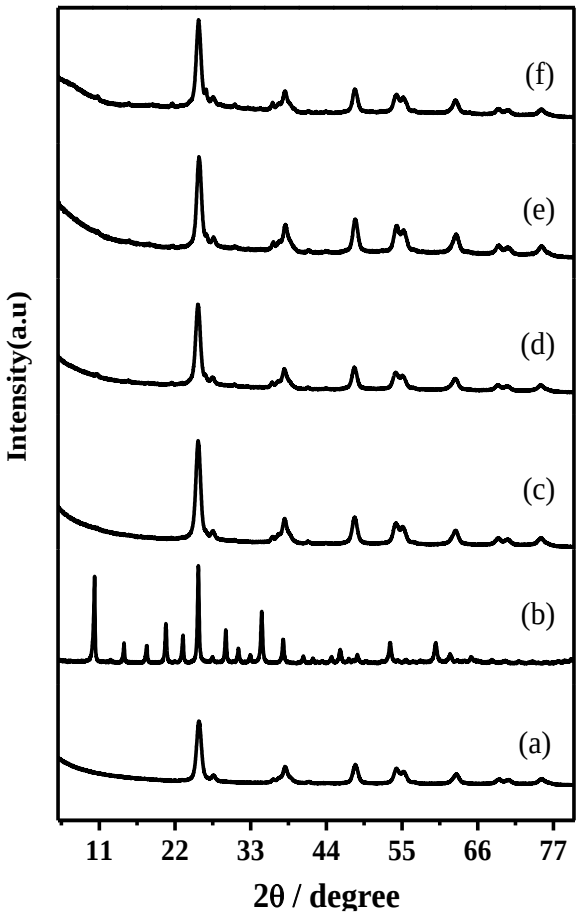

Fig. S2: Samples X-ray diffraction of (a) TiO_2, (b) $H_3PW_{12}O_{40}$, (c) 10 wt% HPW/TiO_2, (d) 15 wt% HPW/TiO_2, (e) 20 wt% HPW/TiO_2, (f) 25 wt% HPW/TiO_2.

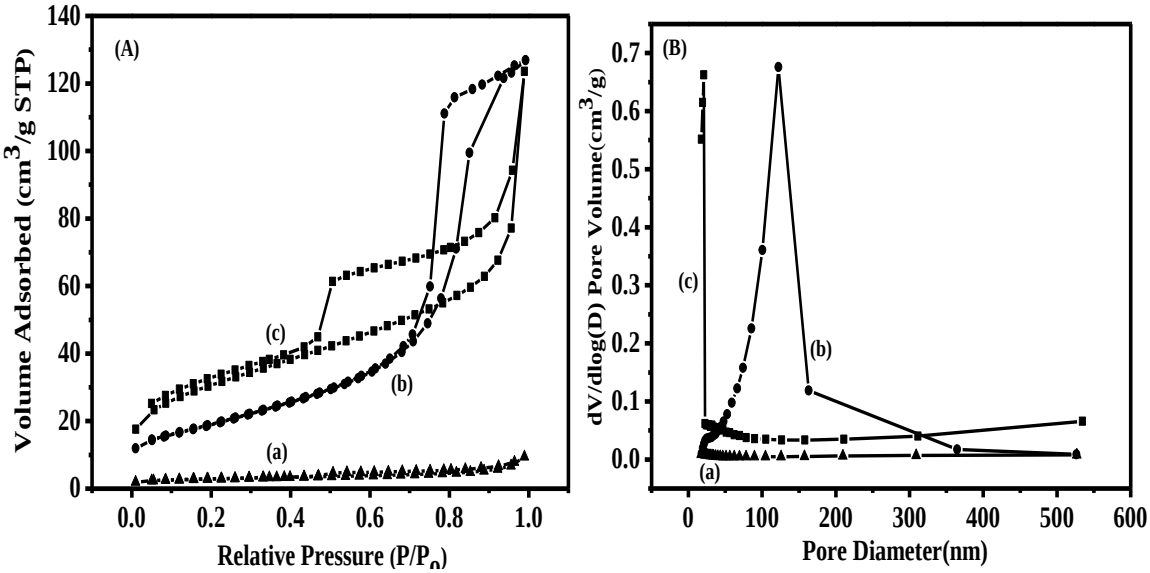

Fig. S3: Nitrogen adsorption-desorption isotherms and their corresponding pore size distribution curves for different metal oxide supported phosphotungstic acid catalysts, (a) 20 wt% HPW/CeO_2, (b) 20 wt% HPW/TiO_2, (c) 20 wt% HPW/ZrO_2.

Fig. S3 showed the nitrogen adsorption-desorption isotherms of 20 wt% HPW/TiO_2, 20 wt% HPW/ZrO_2, 20 wt% HPW/CeO_2 and their corresponding pore size distribution curves. It could be seen from Fig. S3(A) that the nitrogen adsorption-desorption isotherm for phosphotungstic acid catalysts supported by three different metal oxide was a type IV adsorption isotherm of the mesoporous material. Among these isotherms, the adsorption of 20 wt% HPW/TiO_2, 20 wt% HPW/ZrO_2 and 20 wt% HPW/CeO_2 gradually increased with P/P_0 increasing from 0.05 to 0.40. Whereas, for 20 wt% HPW/TiO_2, a large increase in the adsorption occurred at higher P/P_0 = 0.75–0.80, and for 20 wt% HPW/ZrO_2, a small increase in adsorption occurred at P/P_0 = 0.45–0.50, corresponding to the mesoporous materials with large mesopores [32]. This phenomenon was also supported by the pore size distribution of the corresponding sample (Fig. S3(B)), in which 20 wt% HPW/TiO_2 exhibited maximum pore size, indicating that the prepared metal oxide-supported phosphotungstic acid catalyst, especially 20 wt% HPW /TiO_2, had a good specific surface area and void.

The morphology of the bare TiO_2 and 20 wt% HPW/TiO_2 was also investigated. As shown by FE-SEM images in Fig. 1, the bare TiO_2 was composed of very small spheres with a size of about 12-20 nm (Fig. 1a), which was consistent with that reported by Astam K. Patra [38]. In addition, Upon incorporating 20 wt% HPW onto the TiO_2 support (Fig. 1b), the 20 wt% HPW/TiO_2 catalyst still maintained microsphere structure, and the surface of microspheres was rough, indicating that the phosphotungstic acid was uniformly distributed on the surface of TiO_2.

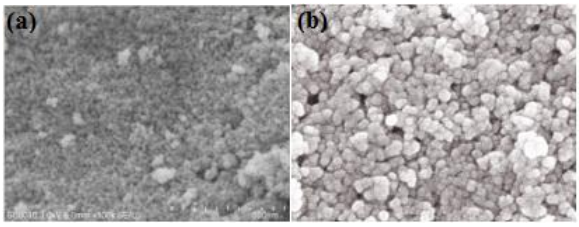

Fig. 1: FE-SEM images of (a) bare TiO_2 and (b) 20 wt% HPW/TiO_2 catalysts.

On the other hand, as probe molecule, trimethylphosphine oxide (TMPO) was used to analysize the acidity of various samples through solid-state ^{31}P MAS NMR, which has been proved to be a stronger and more dependable method for acidity characterization of solid acids [33, 34]. Such ^{31}P-TMPO NMR method based on the fact that the $TMPOH^+$ complex compound formed via the interaction of Brønsted acidic protons (H^+) site in the acid catalyst and probe molecule, whose acidic strengths were linearly correlated with their corresponding ^{31}P NMR chemical shift ($\delta^{31}P$).

Accordingly, Figs. 2 and 3 described the ^{31}P NMR spectra of TMPO adsorbed on various catalysts. As shown in Fig. 2a, the pristine HPW showed extensive resonance at three different regions with δ ^{31}P of –10 to –15, 55 to 75, and 80 to 95 ppm. The signal produced by Keggin polyanions ($PW_{12}O_{40}^{3-}$) of the HPW led to the sharp ^{31}P resonances with δ ^{31}P –10.9 and –15.2 ppm. Owing to TMPO adsorbed on Brønsted acid sites of HPW, with different acidic strengths, peaks with δ ^{31}P in the region of 80–95 ppm were assigned, whereas ^{31}P signal with δ ^{31}P = 67 and 82.8 ppm may be resulted from distorted $(TMPO)_2H^+$ and $TMPOH^+$ adducts, respectively. In terms of TMPO adsorbed on pure TiO_2, overlapping wide signals spanning of 30-60 ppm can be observed (Fig. 2e), which could be attributed to physisorbed TMPO, bulk and mobile TMPO, respectively.

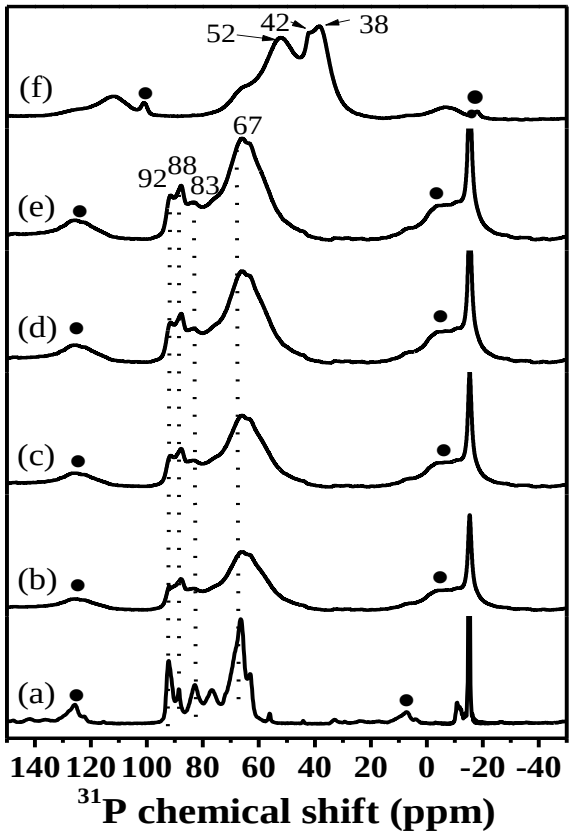

Fig. 2: ^{31}P NMR spectra of different loading HPW on TiO_2 catalysts with TMPO as probe molecule. (a) pure TiO_2, (b) 10 wt% HPW/TiO_2, (c) 15 wt% HPW/TiO_2, (d) 20 wt% HPW/TiO_2, (e) 25 wt% HPW/TiO_2, and (f) pure $H_3PW_{12}O_{40}$. Black dots indicate rotating sidebands.

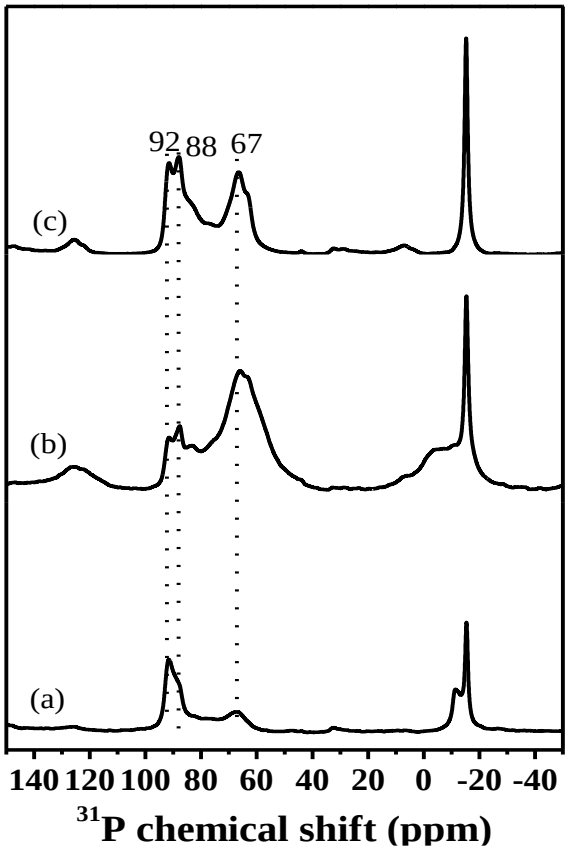

Fig. 3: ^{31}P NMR spectra of HPW supported on different metal oxide catalysts with TMPO as probe molecule. (a) 20 wt% HPW/ZrO_2, (b) 20 wt% HPW/TiO_2, and (c) 20 wt% HPW/CeO_2. Black dots indicate rotating sidebands.

According to the ^{31}P-TMPO NMR approach, a ^{31}P chemical shift value of 86 ppm was predicted for the threshold of superacidity [34, 37, 39, 40]. The existence of the ^{31}P signal with δ ^{31}P = 92.1 and 88.6 ppm in Figs. 2b-e revealed that the pristine HPW and supported HPW/TiO_2 catalysts possessed ultra-strong acidity. From the area of peak (particularly those with δ ^{31}P > 80 ppm), we found that the order of Brønsted acidity for series HPW/TiO_2 catalysts was 25 wt% HPW/TiO_2 > 20 wt% HPW/TiO_2 > 15 wt% HPW/TiO_2 > 10 wt% HPW/TiO_2. Other from the pure HPW, the ^{31}P signal of all laden HPW/TiO_2 catalysts was observed at ca. 67 ppm, indicating the existence of Lewis acidity coming from Ti metal centers. Analogical situation was also found for 20 wt% HPW/ZrO_2 and 20 wt% HPW/CeO_2 catalysts, and the results were illustrated in Fig. 3. The above results implied that the corporation of HPW with metal oxide support tended to trigger formation of Lewis acidity.

Together with high surface area, ultra-strong Brønsted acidity and synergetic effect of Brønsted-Lewis acid of supported HPW/TiO_2 catalysts may be inferred for the superior catalytic activities on the synthesis of benzaldehyde glycol acetal (*vide infra*).

Catalytic activity study

Based on some rules in acid-catalyzed reactions, the level of catalytic activity in acetal reaction is related to the strength of catalyst acidity. Table-1 listed catalytic performances of various catalysts during acetalization of benzaldehyde. As shown in Table-1, Titanium dioxide carrier (TiO_2) with the weakest acidity showed negligible catalytic activity during acetalization of benzaldehyde. Comparing HPW with the strongest Bronsted acid to the titania-loaded catalyst (*x* HPW/TiO_2), it was found that the *x* HPW/TiO_2 (*x* = 10, 15, 20 and 25 wt%) catalysts showed satisfactory catalytic activity. Among the four supported catalysts, the 20 wt% HPW/TiO_2 catalyst exhibited the highest catalytic activity and the acetal yield was 90.1 %. Comparison of the catalytic activity of a series of HPW/TiO_2 catalysts was 20 wt% HPW/TiO_2 > 15 wt% HPW/TiO_2 > 10 wt% HPW/TiO_2 > 25 wt% HPW/TiO_2. Considering the results, we could come to the conclusion that high catalytic activity was related to the strong acidity of *x* wt% HPW/TiO_2 catalyst. However, too much ultra-strong Brønsted acid caused a decrease in acetal yield.

As is shown in Table-1, the results of acetalization of benzaldehyde with glycol using HPW catalyst with different metal oxide support are listed. From Table-1, we found that the 20 wt% HPW/TiO_2 catalyst with large surface area showed the best catalytic activity for acetalization of benzaldehyde. The nature of 20 wt% HPW/TiO_2 catalyst itself acid may also be associated to high acetal yield, which could be confirmed from ^{31}P MAS NMR of adsorbed TMPO (Figs. 2 and 3). The moderate amount of acid sites of Brønsted and Lewis acid of 20 wt% HPW/TiO_2 catalyst was responsible for superior catalytic efficiency. The 20 wt% HPW/TiO_2 catalyst was chosen for subsequent process variable optimization and kinetic studies owing to the best catalytic activity during the experiment of acetalization of benzaldehyde to acetal.

Influence of reaction parameters

The effect of various single factors on acetal reaction was investigated, such as molar ratio of glycol to benzaldehyde, catalyst weight, reaction time, and amount of cyclohexane. The results were displayed in Fig.4. From Fig. 4a, it could be found that yield of benzaldehyde glycol acetal was directly proportional to the amount of glycol, the yield of acetal increased with more amount of glycol. When the molar ratio of glycol to benzaldehyde reached 1.6:1, the yield of benzaldehyde glycol acetal is highest (90.1 %). Since acetalization is a reversible reaction, the excess of glycol made the reactant molecules to collide more easily and resulted in the equilibrium of reaction shifting towards product (i.e., acetal). However, when the molar ratio of glycol to benzaldehyde further increased, the acetal shrinkage decreased, which probably because relative concentration of the 20 wt% HPW/TiO_2 catalyst and benzaldehyde decreased with excess glycol. The result was conformed highly with literature reported earlier [41].

The effect of catalyst amount on acetalization reaction was inspected and the results were listed in Fig. 4b. As shown in Fig. 4b, the acetal yield increased with increasing catalyst amount. When the amount of 20 wt% HPW/TiO_2 catalyst added was 6 %, the maximum acetal yield of 90.1 % was obtained in 3 h. The reason for this phenomenon was that a small amount of catalyst does not have enough active sites for acetalization. Before the amount of catalyst reached 6 %, the number of usable acid moieties increased with the increasing amount of catalyst. Further increasing the catalyst amount beyond 6 wt%, the acetal yield decreased. The selectivity of acetal was damaged by unexpected side-products formed in experiment due to excess acidic sites for excessive amount of catalyst in the reaction. It was speculated that the reaction time was extended, the acetal yield should increase. As shown in Fig. 4c, it could be seen that the acetalization reaction was in equilibrium after 3 hours. The acetal yield remained unchanged when the reaction time was continued to prolong. Low yield was that hemiacetal and/or acetal products may react with water formed during the reaction at prolonged reaction time. Water which was inevitably formed during acetalization reaction shall be removed continuously that was advantageous to increase acetal yield. From the point of view, the role of cyclohexane in the reaction system was to remove water. The acetal yield increased with increasing amount of cyclohexane to reach a maximum of 90.1 % at 12 mL cyclohexane (Fig. 4d). When the amount of cyclohexane exceeded 12 mL, the catalyst system was diluted that reactant concentration and available acid portion of catalyst were reduced, hence, the yield of acetal decreased.

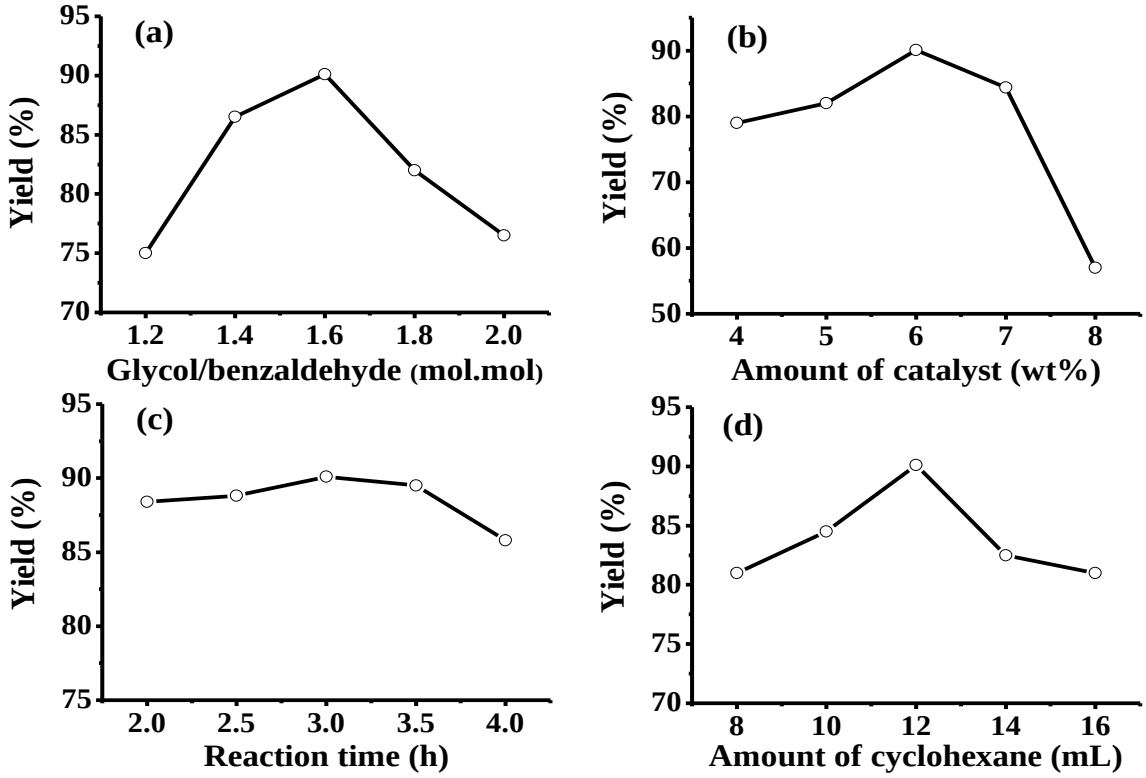

Fig. 4: Effects of different conditions on the yield of acetals during acetalization of benzaldehyde and glycol over 20 wt% HPW/TiO_2 catalyst.

Model fitting and statistical analysis

An analysis of variance (ANOVA) and response surface methodology (RSM) were used to analyze the interaction between the variables in the experiment and optimize the experimental conditions. The independent variables and their levels, real values as well as coded values for the Box-Behnken experimental design were depicted in Table-2. Accordingly, the acetal yield obtained for the acetalization reaction over the 20 wt% HPW/TiO_2 catalyst under various variables and levels were summarized in Table-3, and the response values were predicted by the quadratic model equation:

$$Y = +\ 90.10 - 4.17x_1 + 0.14x_2 + 2.25x_3 + 1.46x_4 - 3.55x_{12} - 4.22x_{22} - 3.98x_{32} - 3.74x_{42} + 1.05x_1x_2 - 1.45x_1x_3 - 1.25x_1x_4 - 0.100x_2x_3 + 4.32x_2x_4 + 3.15x_3x_4 \quad (7)$$

where x_1, x_2, x_3, and x_4 were the encoded values of experimental variables glycol/benzaldehyde molar ratio, reaction time, catalyst weight and amount of cyclohexane, respectively; Y was the acetal yield.

Table-3: Experimental design matrix and measured response values.

Experimental no.					Yield (%)	
	x_1	x_2	x_3	x_4	Experimental	Calculated
1	-1	-1	0	0	87.50	87.40
2	1	-1	0	0	78.00	76.97
3	-1	1	0	0	85.20	85.59
4	1	1	0	0	79.90	79.35
5	0	0	-1	-1	83.00	81.82
6	0	0	1	-1	79.30	80.02
7	0	0	-1	1	79.80	78.44
8	0	0	1	1	88.70	89.24
9	-1	0	0	-1	84.90	84.26
10	1	0	0	-1	78.50	78.43
11	-1	0	0	1	89.40	89.68
12	1	0	0	1	78.00	78.85
13	0	-1	-1	0	78.40	79.41
14	0	1	-1	0	78.80	79.90
15	0	-1	1	0	85.00	84.11
16	0	1	1	0	85.00	84.20
17	-1	0	-1	0	83.00	83.03
18	1	0	-1	0	77.20	77.60
19	-1	0	1	0	90.40	90.43
20	1	0	1	0	78.80	79.20
21	0	-1	0	-1	84.00	84.87
22	0	1	0	-1	76.20	76.50
23	0	-1	0	1	79.00	79.13
24	0	1	0	1	88.50	88.07
25	0	0	0	0	91.00	90.10
26	0	0	0	0	89.80	90.10
27	0	0	0	0	89.50	90.10
28	0	0	0	0	90.50	90.10
29	0	0	0	0	89.70	90.10

The quality of the quadratic model fit (eqn (7)) could be further verified by ANOVA depicted in Table-4. As shown in Table 4, $F = 50.7$, $F > F_{0.01} = 6.71$, and $p < 0.0001$, indicating that the obtained quadratic regression model was extremely significant, i.e., the fitting degree of the model was better in the studied regression region. In addition, the correlation coefficients R^2 and Adj R^2 of model were 0.9807 and 0.9613, respectively, indicating that the linear relationship between the experimental value and the response value was significant, and the feasibility of the model was high. In general, the coefficient of variation, that was used to measure the deviation of each average value, was an important parameter. The smaller the coefficient of variation, the better the repeatability. In this experiment, the coefficient of variation (CV) of the model was 1.17 %, which showed that the designed model has higher credibility and accuracy. Comprehensive comparison of all the above parameters showed that the regression model was reliable and the design of each factor level interval was reasonable. So the model can be used to predict the impact of various factors on the acetal yield.

Therefore, according to predicted model, their corresponding contour plots and curved surface plots were shown in Fig.S4 and Fig.S5, respectively. Fig.S4e and Fig.S5e showed the correlations between x_2 (reaction time) and x_4 (amount of cyclohexane) on acetal yield. It is clear that x_4 has a stronger influence than x_2. Meanwhile, finding that at a reaction time, the acetal yield increased with increasing amount of cyclohexane at first, then the acetal yield dropped significantly with further increasing amount of cyclohexane, a maximum acetal yield was obtained at x_4 = 12 mL. The latter decline in acetal yield was due to the concentration of reactants becomes lower. The same conclusion could be obtained from correlation of x_3x_4 to acetal yield. On the other hand, the correlations between x_1x_2, x_1x_3, x_1x_4 and x_2x_3 to yield of acetal, corresponding to an inferior *P*-value of 0.0497, 0.0102, 0.0228 and 0.8409, respectively. So, x_2, x_3, and x_4 had a very significant effect on the yield of acetal, x_1x_2, x_1x_3, x_1x_4 and x_2x_3 had no significant effect on acetal yield

According to RSM results, the best process variables for acetalization of benzaldehyde with glycol over 20 wt% HPW/TiO_2 catalyst may be derived as: x_1 = 1.43 (molar ratio of glycol to benzaldehyde), x_2 =3.17 h (reaction time), x_3 = 6.77 wt% (amount of catalyst), and x_4 = 13.72 mL (amount of cyclohexane), resulting in a predicted yield of 93.38 % of benzaldehyde glycol acetal. In order to verify the accuracy of these predictions, three parallel experiments were performed at 383 K with $x_1 = 1.4$, $x_2 = 3.2$ h, $x_3 = 6.8$ wt%, $x_4 = 13.7$ mL. Consequently, acetal yields of 93.2 %, 93.5 %, and 92.7 % were acquired which leads to an average experimental yield of 93.1 %. The experimental values were consistent with the predicted values. The above results clearly indicated the effectiveness of the RSM model.

Table-4: ANOVA analysis for the quadratic model of acetal yield.

Source	Sum of squares	DF[a]	Mean squares	*F*	*P* > *F*	Significance[b]
Model	**678.72**	**14**	**48.48**	**50.7**	**< 0.0001**	**
x_1	**208.33**	**1**	**208.33**	**217.89**	**< 0.0001**	**
x_2	**0.24**	**1**	**0.24**	**0.25**	**0.6236**	
x_3	**60.75**	**1**	**60.75**	**63.54**	**< 0.0001**	**
x_4	**25.52**	**1**	**25.52**	**26.69**	**0.0001**	**
x_1^2	**81.94**	**1**	**81.94**	**85.7**	**< 0.0001**	**
x_2^2	**115.33**	**1**	**115.33**	**120.62**	**< 0.0001**	**
x_3^2	**102.71**	**1**	**102.71**	**107.42**	**< 0.0001**	**
x_4^2	**90.81**	**1**	**90.81**	**94.98**	**< 0.0001**	**
$x_1 x_2$	**4.41**	**1**	**4.41**	**4.61**	**0.0497**	*
$x_1 x_3$	**8.41**	**1**	**8.41**	**8.8**	**0.0102**	*
$x_1 x_4$	**6.25**	**1**	**6.25**	**6.54**	**0.0228**	*
$x_2 x_3$	**0.04**	**1**	**0.04**	**0.042**	**0.8409**	
$x_2 x_4$	**74.82**	**1**	**74.82**	**78.26**	**< 0.0001**	**
$x_3 x_4$	**39.69**	**1**	**39.69**	**41.51**	**< 0.0001**	**
Residual	**13.39**	**14**	**0.96**			
Lack of fit	**11.81**	**10**	**1.18**	**2.99**	**0.1514**	**NS**
Pure error	**1.58**	**4**	**0.4**			
total	**692.11**	**28**				

[a]DF = Degree of freedom.

[b] Definition of symbols: * significant; ** highly significant; NS = non-significant.

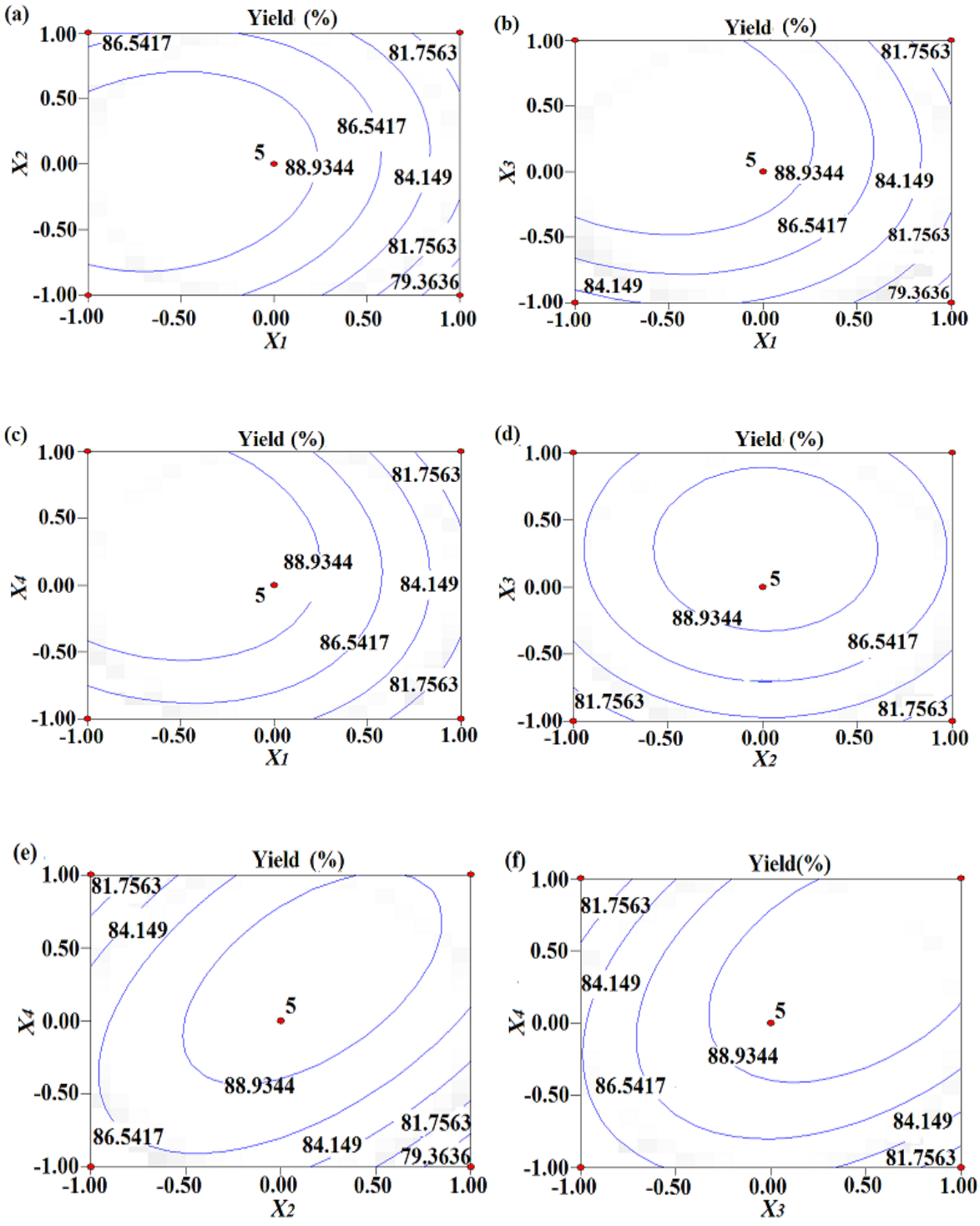

Fig. S4: Contour plots for effects of x_1 vs. x_2 on acetal yield (a), effect of x_1 vs. x_3 on acetal yield (b), effect of x_1 vs. x_4 on acetal yield (c), effect of x_2 vs. x_3 on acetal yield (d), effect of x_2 vs. x_4 on acetal yield (e), and effect of x_3 vs. x_4 on acetal yield (f). The actual and corresponding coded values of each parameter was shown in Table 2.

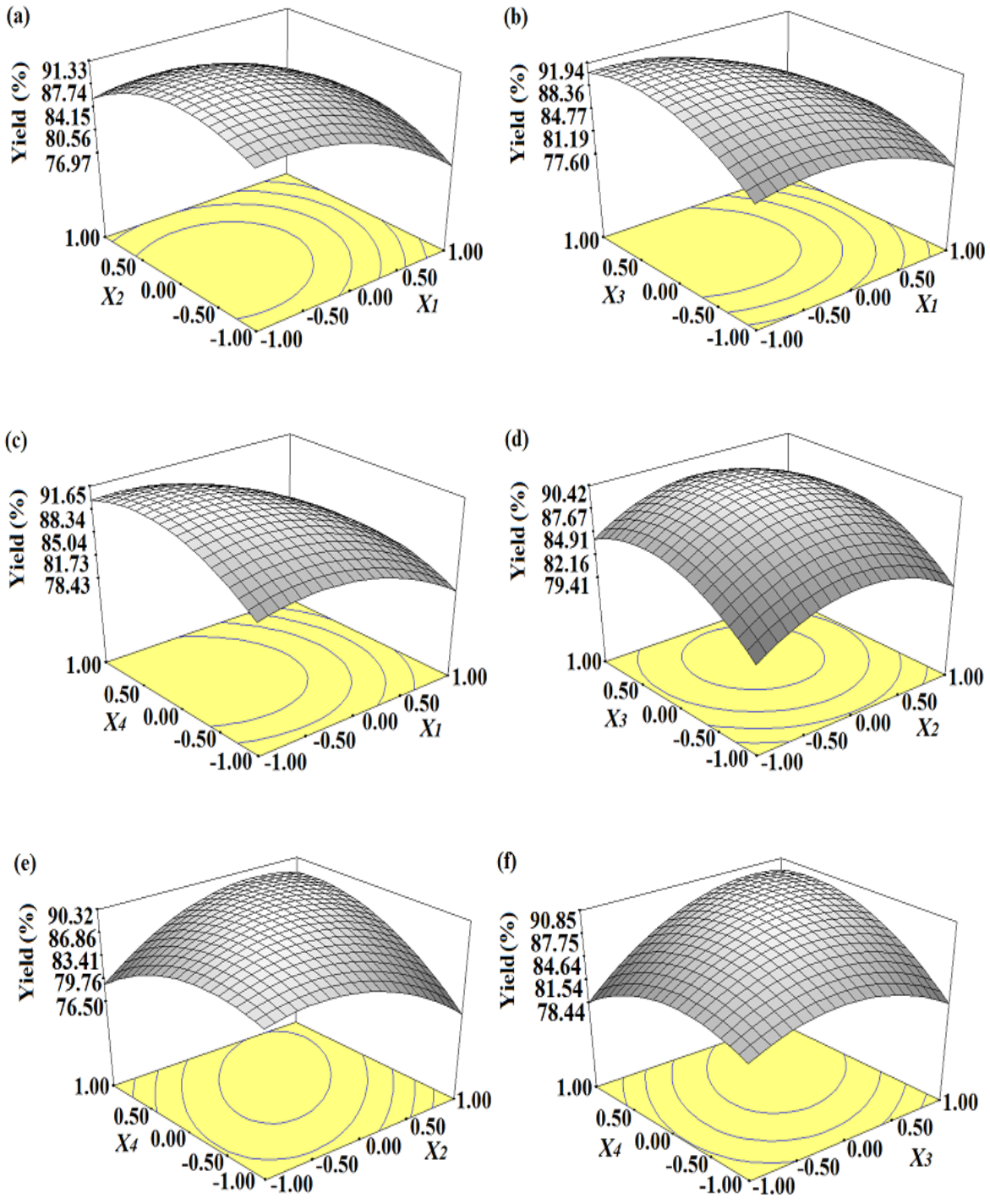

Fig. S5: Surface plots for effects of x_1 vs. x_2 on acetal yield (a), effect of x_1 vs. x_3 on acetal yield (b), effect of x_1 vs. x_4 on acetal yield (c), effect of x_2 vs. x_3 on acetal yield (d), effect of x_2 vs. x_4 on acetal yield (e), and effect of x_3 vs. x_4 on acetal yield (f). The actual and corresponding coded values of each parameter was shown in Table-2.

Stability of the catalyst

As mentioned above, supported catalysts have many advantages, among them, there are easy separation and recycling resistance. In order to verify the stability of the catalyst (20 wt% HPW/TiO_2) in this experiment, we studied the catalyst under the above optimal operating conditions. After each run, the catalyst, that separated from the acetal reaction system, was washed three times with ethyl acetate, then dried in a vacuum drying oven at 70 °C for 10 h before repeated use. As can be seen from Fig. 5, 20 wt% HPW/TiO_2 catalyst had good recovery and reuse. In the experiment of repeated use of catalyst, we repeated the use of catalyst 6 times. The first cycle acetal yield was 93.1 %, and the final production cycle could still reach 90.7 %. The decrease in the acetal yield may be due to the loss of HPW in catalyst resulting in a decrease in catalytic activity. Additional elemental analysis by ICP-OES CID spectrometer revealed that the amount of P element with 0.21 wt% for the fresh catalyst decreased to 0.16 wt% for the sixth spent catalyst. In summary, the 20 wt% HPW/TiO_2 catalyst was suitable and durable for use in acetalization reactions.

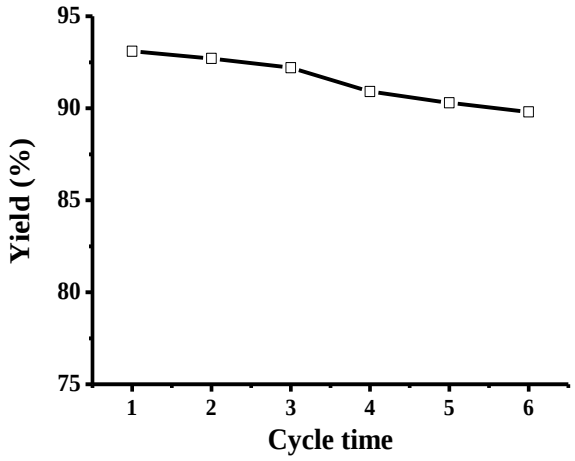

Fig. 5: Recycling tests of the 20 wt% HPW/TiO_2 on the acetalization of benzaldehyde with glycol. (glycol : benzaldehyde molar ratio of 1.4, 6.8 wt% of catalyst, 13.7 mL of cyclohexane, 3.2 h).

Modelling of the kinetic data

In order to establish kinetic model for synthesis of benzaldehyde glycol acetal with 20 wt% HPW/TiO_2 catalyst, the experiment was carried out under reaction conditions optimized by RSM at 363, 373, 383 and 393 K with different time. Other experimental conditions are: molar ratio of glycol to benzaldehyde 1.4:1, 6.8 wt% catalyst (relative to benzaldehyde) and 13.7 mL of cyclohexane. Typically, 1 mL of sample was withdrawn from the reaction mixture for analysis at 30, 60, 90, 120 and 150 min intervals. As a result, the corresponding rate constant based on Eq. (4) during the acetalization reaction under varied concentrations of benzaldehyde (C_A) and glycol (C_B) versus reaction time at various temperatures were recorded. The linear relationship between ln C_A/C_B and t at different temperature for the acetalization was shown in Fig. 6, further indicating that the acetalization of benzaldehyde with glycol was a second-order reaction.

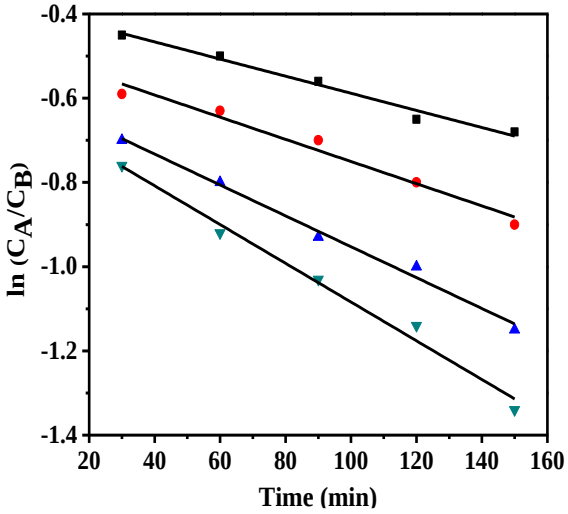

Fig. 6: Plot of ln (C_A/C_B) versus time for acetalization with benzaldehyde and glycol.

Based on eqn (6), a pre-exponential factor k_0 = 3.96 and activation energy Ea = 23.24 kJ mol^{-1} may be derived from the slope and intercept of the Arrhenius plot shown in Fig. 7. Consequently, the kinetic equation for the synthesis benzaldehyde glycol acetal under aforementioned optimal conditions could be readily written as:

$$r = -\frac{dC_A}{dt} = 3.96\exp(-\frac{23.24}{RT})C_A C_B$$

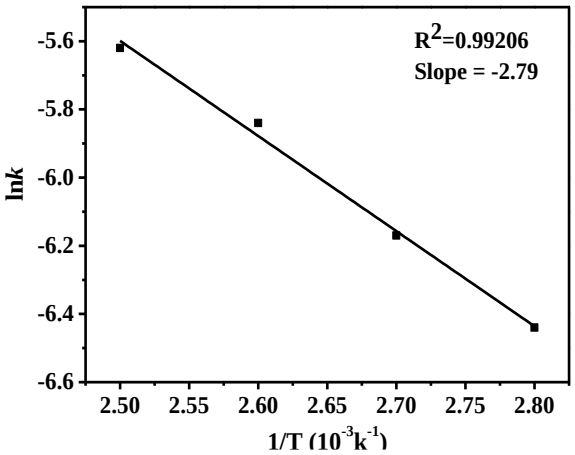

Fig. 7: Arrhenius plot of ln *k* versus 1/T.

The activation energy (*Ea*) observed herein for acetalization over 20 wt% HPW/TiO_2 catalyst is lower than those obtained for the acetalization of *n*-butyraldehyde with glycerol over an Amberlyst-47 ion exchange resin (55.6 kJ/mol) [42], acetalization of acetaldehyde with glycerol over Amberlyst-15 acidic ion exchange resin (51.7 kJ mol^{-1}) [43] and ketalization reaction of acetone with glycerol with H-BEA zeolite (SAR 19) as a catalyst (44.77 kJ mol^{-1}) [44]. The rusluts indicated that 20 wt% HPW/TiO_2 catalyst could be regarded as a high efficiency catalyst for the synthesis of benzaldehyde glycol acetal.

Summary

The complex catalyst that phosphotungstic acid (HPW) loaded onto metal oxides had been successfully prepared and used for acetalization of benzaldehyde with glycol. Among various supported catalysts, the 20 wt% HPW/TiO_2 catalyst showed excellent catalytic activity and acetal yield. Good catalytic properties for composite catalyst may be related to the high surface area, ultra-strong Brønsted acidity and synergetic effect of Brønsted-Lewis acid of catalyst. The optimized reaction conditions based on RSM were as follows: glycol/benzaldehyde molar ratio 1.4:1, catalyst amount 6.8 wt%, reaction time 3.2 h, and 13.7 mL of cyclohexane at 383 K. Consequently, the acetal yield was 93.1 %, which was in good agreement with predicted results. Through recycling research, these eco-friendly and robust catalysts were easily separated and recycled in acetalization reaction. Therefore, the supported 20 wt% HPW/TiO_2 catalysts are cost-effective and can be used to industrial production of benzaldehyde glycol acetal.

Acknowledgment

The supports of this work by the National Key R&D Program of China (2018YFD0400600) and Jiangsu Key Laboratory of Regional Resource Exploitation and Medicinal Research (No. LPRK201701) are gratefully acknowledged.

References

1. D. M. Clode, Carbohydrate cyclic acetal formation and migration, *Chem. Rev*. **79,** 555 (1979).
2. G. Sartori, R. Ballini, F. Bigi, G. Bosica, R. Maggi and P. Righi, Protection (and deprotection) of functional groups in organic synthesis by heterogeneous catalysis, *Chem. Rev*. **104**, 199 (2004).
3. V. M. T. M. Silva and A. E. Rodrigues, Kinetic studies in a batch reactor using ion exchange resin catalysts for oxygenates production: Role of mass transfer mechanisms, *Chem. Eng. Sci*. **61**, 316 (2006).
4. R. J. Linderman and S. Chen, Diastereoselective addition of alkynylstannanes to alpha stannyl substituted mixed acetals: Synthesis of precursors for allenyl carbinols., *Tetrahedron Lett.* **37**, 3819 (1996).
5. H. Nemoto, K. Tanimoto, Y. Kanao, S. Omura and Y. Kita, Protecting-group-free catalytic asymmetric total synthesis of (−)-rosmarinecine, *Tetrahedron*, **68**, 7295 (2012).
6. S. P. Chopade and M. M. Sharma, Reaction of ethanol and formaldehyde: use of versatile cation-exchange resins as catalyst in batch reactors and reactive distillation columns, *React. Funct. Polym*. **32**, 53 (1997).
7. P. R. Verma, S. Mandal, P. Gupta and B. Mukhopadhyay, ChemInform Abstract: Carbohydrate derived thiosemicarbazone and semicarbazone palladium complexes: Homogeneous catalyst for C-C cross coupling reactions, *Tetrahedron Lett*. **54**, 4914 (2013).
8. F. Frusteri, L. Spadaro, C. Beatrice and C. Guido, Oxygenated additives production for diesel engine emission improvement, *Chem. Eng. J*. **134**, 239 (2007).
9. N. Gupta, Sonu, G. L. Kad and J. Singh, Acidic ionic liquid [bmim]HSO_4: An efficient catalyst for acetalization and thioacetalization of carbonyl compounds and their subsequent

deprotection, *Catal. Commun*. **8**, 1323 (2007).
10. X. X. Han, W. Yan, K. K. Chen, C. T. Hung, L. L. Liu, P. H. Wu, S. J. Huang and S. B. Liu, Heteropolyacid-based ionic liquids as effective catalysts for the synthesis of benzaldehyde glycol acetal, *Appl. Catal. A-Gen*. **485**, 149 (2014).
11. Y. L. Hu, S. Zheng and F. M. Zhang, Fabrication of MIL-100 (Fe) @ SiO_2 @ Fe_3O_4 core-shell microspheres as a magnetically recyclable solid acidic catalyst for the acetalization of benzaldehyde and glycol, *Front. Chem. Sci. Eng*. **10**, 534 (2016).
12. D. L. Long, R. Tsunashima and L. Cronin, Polyoxometalates: building blocks for functional nanoscale systems, *Chem. Int. Ed*. **49**, 1736 (2010).
13. G. A. Tsigdinos, Heteropoly compounds of molybdenum and tungsten, Top. *Curr. Chem*. **76**, 1 (1978).
14. L. C. W. Baker and D. C. Glick, Present general status of understanding of heteropoly electrolytes and a tracing of some major highlights in the history of their elucidation, *Chem. Rev*. **98**, 3 (1998).
15. I. V. Kozhevnikov, Catalysis by heteropoly acids and multicomponent polyoxometalates in liquid-phase reactions, *Chem. Rev*. **98**, 171 (1998).
16. N. Mizuno and M. Misono, Heterogeneous catalysis, *Chem. Rev*. **98**, 199 (1998).
17. C. Srilakshmi, N. Lingaiah, I. Suryanarayana, P. S. Sai. Prasad, K. Ramesh and B. G. Anderson, In situ synthesis of ammonium salt of 12-molybdophosphoric acid on iron phosphate and the ammoxidation functionality of the catalyst in the transformation of 2-methylpyrazine to 2-cyanopyrazine, *Appl. Catal. A: Gen*. **296**, 54 (2005).
18. P. M. Rao, A. Wolfson, S. Kababya, S. Vega and M. V. Landau, Immobilization of molecular $H_3PW_{12}O_{40}$ heteropolyacid catalyst in alumina-grafted silica-gel and mesostructured SBA-15 silica matrices, *J. Catal*. **232**, 210 (2005).
19. P. Ferreira, I. M. Fonseca, A. M. Ramos, J. Vital and J. E. Castanheiro, Esterification of glycerol with acetic acid over dodecamolybdophosphoric acid encaged in USY zeolite, *Catal. Commun*. **10**, 481 (2009).
20. M. B. Xu, J. Yang, Y. K. Huang and S. J. Yang, Catalytic synthesis of butyraldehyde glycol acetal with $H_4SiW_{12}O_{40}$/MCM-48, *Adv. Mater. Res*. **531**, 312 (2012).
21. X. X. Han, Y. Y. Kuang, C. H. Xiong, X. J. Tang, Q. Chen, K. W. Wang, C. T. Huang, L. L. Liu and S. B. Liu, Brazil, Heteropoly tungstate supported on metal oxide catalysts for liquid phase oxidation of benzyl alcohol with hydrogen peroxide, *J. Braz. Chem. Soc*. **29**, 88 (2018).
22. R. P. Dong, J. H. Choi, S. Park and I. K. Song, Reduction potential, UV-visible absorption edge energy, and oxidation catalysis of niobium-containing $H_{3+x}PW_{12-x}Nb_xO_{40}$ Keggin and $H_{6+x}P_2W_{18-x}Nb_xO_{62}$Wells-Dawson heteropolyacid catalysts, *Appl. Catal. A: Gen*. **394**, 201 (2011).
23. S. S. Wang, J. Zhang, C. L. Zhou, G. Vo-Thanh and Y. Liu, An ionic compound containing Ru(III)-complex cation and phosphotungstate anion as the efficient and recyclable catalyst for clean aerobic oxidation of alcohols, *Catal. Commun*. **28**, 152 (2012).
24. S. Pathan and A. Patel, Solvent free clean selective oxidation of alcohols catalyzed by mono transition metal (Co, Mn, Ni)-substituted Keggin-phosphomolybdates using hydrogen peroxide, *Appl. Catal. A. Gen*. **459**, 59 (2013).
25. H. Atia, U. Armbruster and A. Martin, Dehydration of glycerol in gas phase using heteropolyacid catalysts as active compounds, *J. Catal*. **258**, 71 (2008).
26. M. A. Schwegler, P. Vinke, M. van. Der. Eijk and H. van. Bekkum, Activated carbon as a support for heteropolyanion catalysts, *Appl. Catal. A: Gen*. **80**, 41 (1992).
27. P. Madhusudhan. Rao, A. Wolfson, S. Kababya, S. Vega and M. V. Landau, Immobilization of molecular $H_3PW_{12}O_{40}$ heteropolyacid catalyst in alumina-grafted silica-gel and mesostructured SBA-15 silica matrices, *J. Catal*. **232**, 210 (2005).
28. A. Ghanbari-Siahkali, A. Philippou, J. Dwyer and M. W. Anderson, The acidity and catalytic activity of heteropoly acid on MCM-41 investigated by MAS NMR, FTIR and catalytic tests, Appl. Catal. A: Gen. **192**, 57 (2000).
29. Y. Izumi and K. Urabe, Catalysis of heteropoly acids entrapped in activated carbon, *Chem. Lett*. **5**, 663 (1981).
30. B. Sulikowski, J. Haber, A. Kubacka, K. Pamin, Z. Olejniczak and J. Ptaszyn. ski, Novel "ship-in-the-bottle" type catalyst: evidence for encapsulation of 12-tungstophosphoric acid in the supercage of synthetic faujasite, *Catal. Lett*. **39**, 27 (1996).
31. A. K. Patra, A. Dutta and A. Bhaumik. Highly ordered mesoporous TiO_2−Fe_2O_3 mixed oxide

synthesized by sol−gel pathway: An efficient and reusable heterogeneous catalyst for dehalogenation reaction, ACS *Appl. Mater. Interfaces*. **4**, 5022 (2012).

32. S. H Zhu, Y. L. Zhu, X. Q. Gao, T. Mo, Y. F. Zhu, Y. W. Li, Production of bioadditives from glycerol esterification over zirconia supported heteropolyacids, *Bioresour. Technol*. **130**, 45 (2013).
33. A. Zheng, S. Li, S. B. Liu and F. Deng, Acidic properties and structure-activity correlations of solid acid catalysts revealed by solid-state NMR spectroscopy, Acc. *Chem. Res*. **49**, 655 (2016).
34. A. Zheng, S. J. Huang, W. H. Chen, P. H. Wu, H. Zhang, H. K. Lee, L. C. de Ménorval, F. Deng and S. B. Liu, ^{31}P Chemical shift of adsorbed trialkylphosphine oxides for acidity characterization of solid acids catalysts, *J. Phys. Chem. A*. **112**, 7349 (2008).
35. X. X. Han, K. K. Chen, W. Yan, C. T. Hung, L. L. Liu, P. H. Wu, K. C. Lin and S. B. Liu, Amino acid-functionalized heteropolyacids as efficient and recyclable catalysts for esterification of palmitic acid to biodiesel, *Fuel*. **165**, 115 (2016).
36. P. M. Rao, A. Wolfson, S. Kababya, S. Vega and M. V. Landau, Immobilization of molecular $H_3PW_{12}O_{40}$ heteropolyacid catalyst in alumina-grafted silica-gel and mesostructured SBA-15 silica matrices, *J. Catal*. **232**, 210 (2005).
37. S. J. Huang, C. Y. Yang, A. Zheng, N. Feng, N. Yu, P. H. Wu, Y. C. Chang, Y. C. Lin, F. Deng and S. B. Liu, New insights into Keggin-type 12-tungstophosphoric acid from ^{31}P MAS NMR analysis of absorbed trimethylphosphine oxide and DFT calculations, *Chem. Asian J*. **6**, 137 (2011).
38. A. K. Patra, S. K. Das and A. Bhaumik. Self-assembled mesoporous TiO_2 spherical nanoparticles by a new templating pathway and its enhanced photoconductivity in the presence of an organic dye, *J. Mater. Chem*. **21**, (2011).
39. A. Zheng, S. J. Huang, S. B. Liu and F. Deng, Acid properties of solid acid catalysts characterized by solid-state ^{31}P NMR of adsorbed phosphorous probe molecules, Phys. Chem. Chem. Phys. **13**, 14889 (2011).
40. A. Zheng, H. Zhang, X. Lu, S. B. Liu and F. Deng, Theoretical predictions of ^{31}P NMR chemical shift threshold of trimethylphosphine oxide absorbed on solid acid catalysts, J. Phys. Chem. B. **112**, 4496-4505 (2008).
41. X. X. Han, K. Ouyang, C. H. Xiong, X. J. Tang, Q. Chen, K. W. Wang, L. L. Liu, C. T. Hung and S. B. Liu, Transition-metal incorporated heteropolyacid-ionic liquid composite catalysts with tunable Brønsted/Lewis acidity for acetalization of benzaldehyde with ethylene glycol, *Appl. Catal. A: Gen*. **543**, 115 (2017).
42. M. B. Güemez, J. Requies, I. Agirre, P. L. Arias, V. L. Barrio and J. F. Cambra, Acetalization reaction between glycerol and n-butyraldehyde using an acidic ion exchange resin. Kinetic modelling, *Chem. Eng. J*. **228**, 300 (2013).
43. R. P. V. Faria, C. S. M. Pereira, V. M. T. M. Silva, J. M. Loureiro and A. E. Rodrigues, Glycerol valorization as biofuel: Thermodynamic and kinetic study of the acetalization of glycerol with acetaldehyde, *Ind. Eng. Chem. Res*. **52**, 1538 (2013).
44. V. Rossa, Y. S. P. Pessanha, G. C. Diaz, L. D. T. Camara, S. B. C. Pergher and D. A. G. Aranda, Reaction kinetic study of solketal production from glycerol ketalization with acetone, *Ind. Eng. Chem. Res*. **56**, 479 (2017).